Ocean acidification reduces mechanical properties of the Portuguese oyster shell with impaired microstructure: a hierarchical analysis

Yuan Meng[1], Zhenbin Guo[2], Susan C. Fitzer[3], Abhishek Upadhyay[1], Vera B. S. Chan[4], Chaoyi Li[1], Maggie Cusack[5], Haimin Yao[2], Kelvin W. K. Yeung[6] and Vengatesen Thiyagarajan[1]

[1]The Swire Institute of Marine Sciences and School of Biological Sciences, The University of Hong Kong, Pokfulam, Hong Kong, China.

[2]Department of Mechanical Engineering, The Hong Kong Polytechnic University, Hung Hom, Kowloon, Hong Kong, China

[3]Institute of Aquaculture, Faculty of Natural Sciences, University of Stirling, Pathfoot Building, Stirling, FK9 4LA, UK

[4]Department of Biological Sciences, Clemson University, SC, USA

[5]Division of Biological & Environmental Sciences, Faculty of Natural Sciences, University of Stirling, Cottrell Building, Stirling, FK9 4LA, UK

[6]Department of Orthopaedics and Traumatology, Queen Mary Hospital, The University of Hong Kong, Pokfulam, Hong Kong, China.

Correspondence to: V. Thiyagarajan (rajan@hku.hk)

Abstract. The rapidly intensifying process of ocean acidification (OA) in coastal areas due to anthropogenic CO_2 is not only depleting carbonate ions necessary for calcification but also causing acidosis and disrupting internal pH homeostasis in several marine organisms. These negative consequences of OA on marine communities, particularly to shellfish oyster species, has been very well documented in recent studies, however, the consequences of these reduced or impaired calcification processes on the end-product, shells or skeletons, still remains one of the major research gaps. Shells produced by marine organisms under OA are expected to be corroded with disorganized or impaired crystal orientation or microstructures with reduced mechanical property. To bridge this knowledge gap and to test the above hypothesis, we investigated the effect of OA on shell of the commercially important oyster species (*Crassostrea angulata*) at ecologically and climatically relevant OA levels (using pH 8.1, 7.8, 7.5, 7.2 as proxies). In decreased pH conditions, a drop of shell hardness and stiffness was revealed by nanoindentation tests, while an evident loosened internal microstructure was detected by scanning electron microscopy (SEM). In contrary, the crystallographic orientation of oyster shell showed no significant difference with decreasing pH by Electron Back Scattered Diffraction (EBSD) analyses. These results indicate the loosened internal microstructure may be the cause of the OA induced reduction in shell hardness and stiffness. Micro-computed tomography analysis (Micro-CT) indicated that an overall "down-shifting" of mineral density in the shell with decreasing pH, which implied the loosened internal microstructure may run through the shell, thus inevitably limiting the effectiveness of the shell defensive function. This study surfaces potential bottom-up deterioration induced by OA on oyster shells, especially in their early juvenile life stage. This knowledge is critical to forecast the survival and production of edible oysters in future ocean.

1 Introduction

Edible oysters belong to the genus "*Crassostrea*" have a complex life cycle, in which the free-swimming larvae attach onto a suitable hard substrate and then metamorphose into sessile juveniles within a few hours (Medaković et al., 1997). The oyster larval shell is primarily made of aragonite, a denser and mechanically stronger form of calcium carbonate ($CaCO_3$) compared to calcite, which is a stable but brittle polymorphous $CaCO_3$. Upon metamorphosis, the fraction of calcite rapidly increases

and becomes the main component in the juvenile and adult oyster shell (Medaković et al., 1997; Weiner and Addadi, 1997).

40   The composition of the mineral polymorphs and the occluded organic matrix contribute to a wide array of fascinating hierarchical composites, which determine the mechanical strengths of shell structures in each of these life stages (Lee et al., 2011). These early-life stages of marine invertebrates, including oysters, are highly vulnerable to predators (Newell et al., 2007) and environmental stressors (Thomsen et al., 2015) when compared to the adult stages. Production of mechanically stronger and structurally integrated shells during larval and juvenile period, therefore, is essential to accomplish the post-

45   larval phase because their shell integrity and strength protect them shell-breaking and drilling predators.

The oceans currently absorb about a third of man-made CO_2, which dissolves in seawater forming carbonic acid and increases the seawater acidity, known as ocean acidification (OA). A meta-analysis showed that the calcification rate of marine organisms, including oysters, is highly vulnerable to high-pCO_2 driven decreases in seawater pH (Feely et al., 2009; De Bodt et al., 2010). If the early-life stages of edible oysters are vulnerable to this near-future OA process, then it could

50   directly harm oyster survival and their aquaculture production. There is already evidence of the negative effects of OA; for example, spat production in oyster hatcheries on the west coast of USA has started to decline, partially due to poorly calcified larval shells under upwelled high-CO_2 waters (Barton et al., 2012). Previous studies on calcifying organisms, including oysters, suggest that OA not only reduces calcification rates, but also increases dissolution of formed shells (Ries, 2011; Bednarsek et al., 2012). The decreased pH depletes carbonate ions necessary for $CaCO_3$ mineralization chemically, as

55   well as weakens marine organisms physiologically by causing acidosis and impairing internal pH homeostasis needed for optimal calcification (Dupont and Portner, 2013) . Recently, an increasing number of studies capture the importance of the mechanical properties of calcareous shell, the end-products of calcification, under OA scenario (Dickinson et al., 2012; Ivanina et al., 2013; Li et al., 2014; Fitzer et al., 2015; Collard et al., 2016; Teniswood et al., 2016; Milano et al., 2016). For instance, it has been reported that the Pacific oyster and the Eastern oyster produced softer shells with reduced

60   mechanical strength under OA condition (Beniash et al., 2010; Dickinson et al., 2012). Despite these OA threats to oyster calcification process, studies are yet to demosntrate the hierarchical structural organization of oyster shells under elevated CO_2 and OA conditions. Importantly, the modulating effect of OA on the inherent relationship between shell strctural and mechanical features is yet to be studied in detail.

This study is designed specifically to fill this gap in our current knowledge using the ecologically and economically

65   important edible oyster (*Crassostrea angulata*) as model species. Here, the quantitative relationship between microstructural and mechanical properties was examined using the newly formed juvenile oyster shells. Specifically, the effect of OA on this relationship was tested using three levels of environmentally and climatically relevant levels of high-CO_2 induced decreased pH. As the calcitic foliated layer is the major shell structure for mechanical support in oysters (Lee et al., 2008), we specifically examined its structural and mechanical properties by using variety of materials science techniques such as

70   scanning electron microscopy (SEM), crystallography by electron backscatter diffraction (EBSD) and nanoindentation tests. To further evaluate the overall structural integrity, we quantified shell mineral density, mineral density-volume ratio relationships using high-resolution micro-computed tomography scanning (Micro-CT).

2 Materials and methods

2.1 Experimental animal and design

75   Sexually matured adult oysters of the Portuguese oyster species, *Crassostrea angulata,* were collected from the coastal area in Fujian, China (26°05′53.36″N 119°47′45.81″W) in the South China Sea on July 29th, 2014. The adults were transported to the laboratory at the Swire Institute of Marine Science (SWIMS), The University of Hong Kong. They were acclimated in

flow-through tanks in natural seawater at ambient conditions (31 psu salinity, 29 °C and pH$_{(NBS)}$ 8.1) for a week. They were fed with a mixed algae diet (*Isochrysis galbana* and *Chaetoceros gracilis*). Sperm and eggs were obtained from more than 10
80   males and 10 females by the "strip spawning" method (Dineshram et al., 2013), and cultured under ambient conditions. After 24 h postfertilization, embryos developed into D-shaped veliger larvae. Larvae were subjected to pH perturbation to study the effects of ocean acidification (OA) process on oyster shell structure and mechanical features in the early stages of development.

        Four environmentally and climatically relevant pH levels (pH 8.1, 7.8, 7.5, and 7.2) were selected as proxies to
85   investigate the effect of CO$_2$-driven OA on oyster shells. According to IPCC projections, the average pH of oceans (currently pH 8.1) is expected to drop to pH 7.8 and 7.5 by the year 2100 and 2300, respectively (Feely et al., 2009). The very low pH 7.2 treatment was included in this study to understand the impact of extreme environmental conditions in the coastal habitats of *C. angulata*, where seawater pH naturally fluctuates and may decrease by as much as 0.8 units due to river runoff and microbial respiration (Duarte et al., 2013; Thiyagarajan and Ko, 2012). Treatment pH levels were maintained by bubbling
90   filtered natural seawater with air enriched with CO$_2$ at the required concentrations using gas flow meters/controllers (Cole-Parmer, USA). Oyster larvae were raised from the D-shaped veliger stage to the juvenile stage under the four pH levels with four biologically independent replicates tanks for each treatment. Briefly, D-shaped larvae (10 larvae/mL, 50L replicate tanks, 1 μm FSW, 31 psu salinity, at 29°C ± 2°C) were reared until the pediveliger stage following previously described methods (Dineshram et al., 2013). After about 2 to 3 weeks, larvae attained competency for attachment and metamorphosis.
95   They were transferred from each 50 L replicate tanks to 1 L replicate tanks containing plastic substrates coated with 7-day-old natural biofilms. Attachment and metamorphosis took place within 24 h, and attached oyster were reared in 1 L replicate tanks with the same pH level before attachment for 35 days until shell collection for subsequent analysis. Larvae and juveniles were fed twice a day using mixture of live *Isochrysis galbana* and *Chaetoceros gracilis* (5-10×10⁶ cells/mL, 1:1 ratio). Seawater pH (NBS scale) and the temperature were measured using a Metter-Toledo (SG2) probe and salinity with a
100   refractometer (ATAGO, S/Mill0E; Japan). The probe was calibrated using NIST buffers (pH =4.01, 7.00, and 9.21; Mettler Toledo, Gmbh Analytical CH8603 Schwerzenbach, Switzerland). In each culture, tanks levels of pH, temperature and salinity were measured daily. Daily measurements were firstly averaged within and among days per each replicate tank. Afterwards, the treatment level (Mean ± SD; Table S1) was calculated, by averages of the replicate culture tanks within each treatment (n = 4). Samples of seawater (50 ml) from each culture tank were collected every 4 days and poisoned with 10 μl
105   of 250 mM mercuric chloride for total alkalinity (TA) analysis using the Alkalinity Titrator (AC-A2, Apollo SciTech's Inc., U.S.). The TA measurement was standardized with a certified seawater reference material (Batch 106, A.G. Dickson, Scripps Institution of Oceanography, U.S.). The carbonate system parameters, i.e. carbon dioxide partial pressure (*p*CO$_2$; μatm), carbonate ion concentration (CO$_3$$^{2-}$; μmol kg^{-1}), calcite and aragonite saturation state (Ω_{Ca}, Ω_{Ar}), were calculated using the CO2SYS software program (Pierrot et al., 2006) with equilibrium constants K$_1$, K$_2$ and KSO$_4$ (Mehrbach et al.,
110   1973; Dickson and Millero, 1987) (Table S1). On the 35th day post-metamorphosis, juveniles were sacrificed and preserved in 75% ethanol for the following analyses.

2.2 Shell microstructure analysis

The sessile juvenile oyster permanently cements the left valve of its shell to substratum, whereas its right valve provides protection from predators and the environment. In this study, only the right valve was used in the shell analysis. The surface
115   topography of the intact shell was examined under variable pressure at 30 kV using a scanning electron microscope (SEM; Hitachi S-3400N VP SEM, Hitachi, Japan). To examine sectional surface microstructures, shells were embedded in epoxy resin (EpoxyCure, Buehler) and sliced along the dorsal-ventral axis using a diamond trim saw blade. This allows for a more

controlled comparison between the hinge region and the middle region of the shell. The hinge region (hereafter also referred to as "older shell") is the part of the shell that is deposited first by the juvenile oyster, whereas the middle region (hereafter also referred to as "younger shell") is the part of the shell that is deposited more recently. The bill region, formed most recently, was not included in this study because it is too fragile to handle. The sectioned surfaces were polished for 2 to 5 min using grit papers (P320, P800, P1200, P2500, and P4000) and etched for 20 seconds using 1% acetic acid, and then washed with distilled water and air dried. The sectioned resin blocks were mounted on aluminium stubs using carbon adhesive tape with the polished side up. The area surrounding the specimen was painted with silver to reduce charge build-up, and the sectioned surfaces were sputter-coated with 50-nm thick gold−palladium alloy. The shell microstructures were examined under an accelerating voltage of 5 kV using a LEO 1530 Gemini FSEM (Zeiss, Germany). The cross-sectional porosity of foliated laminated structure was calculated using ImageJ software by standardizing and converting an SEM image to thresholding. The pore area was then calculated by using the ImageJ "Analyse Particles" feature due to the divergence in the size of pores. The pores area was sized with a confidence area of greater than 0.001 µm^2. Three to four specimens from each treatment were randomly selected and examined (n = 3~4). All data was tested for normality of residuals, normality, and homogeneity of variance before analysing by ANOVA. Student-Newman-Keuls test was used to compare the means following one-way ANOVA.

2.3 Shell crystallography analysis

Shell crystallographic orientation was analysed by Electron Backscatter Diffraction (EBSD). Shells were prepared according to the above method, but without etching. The shell surfaces were ultra-polished for 4 min using cloths with 1 µm and 0.3 µm Alpha alumina powders and for 2 min using colloidal silica. In order to investigate both larva aragonite and juvenile calcite composition, an area throughout the sectional surface of the older hinge regions were selected. The EBSD analyses were carried out under low vacuum mode (~50 Pa) with a beam voltage of 20 kV using an FEI Quanta 200F with the stage tilted at 70° to examine backscatter Kikuchi patterns (Perez-Huerta and Cusack, 2009). Diffraction intensity, phase, and crystallographic orientation maps were produced using the OIM Analysis 6.2 software. Data was partitioned through two clean-up procedures to display grains with a confidence index (CI) greater than 0.1. Pole figures were used to illustrate the spread of crystallographic orientation (Perez-Huerta and Cusack, 2009). The colours in the crystallographic orientation maps and pole figures were used to quantify the crystallographic orientation. Two randomly selected specimens were examined per treatment.

2.4 Shell mechanical properties analysis

After SEM and EBSD analysis, the resin blocks were re-polished for 5 min using grit papers (P2500 and P4000) and for another 5min using cloth with colloidal silica to remove the gold-palladium coating and etched shell surface. The mechanical properties of the polished longitudinal cross sections were determined by measuring the hardness (H) and stiffness (E) using load and displacement sensing nanoindentation tests (Perez-Huerta et al., 2007). Hardness and stiffness of foliated layers were measured in the older hinge and younger middle regions of the specimens used in the SEM analysis. The nanoindentation tests were carried out from the interior to the exterior shell in these regions at ambient temperature with a Hysitron TriboIndenter TI 900 (TI 900, Hysitron, MN, USA) equipped with a Berkovich indenter (with a half-angle of 63.5°). Indentations were made in each specimen using a 6−11 indent-per-row pattern and a maximum load of 2000 µN with valid contact depth of 16 to 184 nm. The hardness and stiffness from each indentation were obtained from the loading-unloading curve using the Oliver-Pharr model (Doerner and Nix, 1986; Oliver and Pharr, 1992). Five to six specimens of each treatment were randomly selected for nanoindentation tests. Measurements were firstly averaged within per specimen

and then per replicate tank. Finally, three to four replicate values per treatment were compared (n = 3~4). All data was tested for normality of residuals, normality, and homogeneity of variance before analysing by ANOVA. Student-Newman-Keuls test was used to compare the means following one-way ANOVA.

160 **2.5 Shell mineral density analysis**

The three-dimensional shell density maps, the overall mineral density and the mineral density-volume ratio relationships were obtained using a high-resolution micro-CT scanning system (SkyScan 1076, Skyscan, Kontich, Belgium) with a spatial resolution of 9 μm. Individual shells were placed in a small plastic container held securely in the chamber of the micro-CT scanner. Shell densities and volume ratios of partial density were calculated by relative comparison using standardized

165 phantoms used for bone density measurement in the analytical software CT-Analyser v 1.14.4.1 (SkyScan) (Celenk and Celenk, 2012). The 3D digital data was converted from ~1000 2D layers using reconstruction software CT-Volume v 2.2.1.0 (SkyScan). Three randomly selected specimens were used per treatment (n = 3). The volume ratio with partial density ranges of 0 to 0.5 g/cm^3, 0.5 to 1 g/cm^3, and >1.5 g/cm^3, and density of the treatment groups were compared with the controls by one-way ANOVAs. For the datasets that did not meet the requirement of variance homogeneity, i.e., the volume ratio with a

170 partial density range of 1 to 1.5 g/cm^3, Kruskal-Wallis tests were used to compare the effect of pH on these shell properties. For all other datasets, Student-Newman-Keuls test was used to compare the means following one-way ANOVA. Otherwise, Dunn's test was used after Kruskal-Wallis test. Linear regressions (Volume ratio (%) = b× mineral density (g/cm^3) +a) was utilized to determine the relationships between mineral density and volume ratio, a is the y-intercept and b is the scaling exponent of consumption. To compare slopes of the resulting linear models, analysis of covariance (ANCOVA) was

175 performed by using log_{10} transformed volume ratio as the dependent variable, pH levels as the independent variable, and mineral density range as covariates. All data met the homogeneity of variance and normality assumptions of parametric tests. ANCOVA were implemented in R 3.3.2 using the statistical package Linear and Nonlinear Mixed Effects Models (Team, 2013).

3 Results

180 **3.1 Deceased pH alters shell surface and internal microstructure**

As shown by the SEM, decreased pH altered both shell topography (Fig. 1) and internal microstructure (Fig. 2). Mineral dissolution or erosion was prominent on the outer surface layers of shells under decreased pH. The shells of juveniles raised at pH 7.8 (Fig. 1b, f) and pH 7.5 (Fig. 1c, g) showed signs of erosion or physical damage when compared to the controls (Fig. 1a, e). At the lowest pH of 7.2 with undersaturated calcite conditions, the outer prismatic layer was completely absent

185 at the older hinge and younger middle regions of the shell (Fig. 1d, h). Though the overall calcitic foliated laminas alignment were retained, those in the shells of untreated juveniles (controls) were compactly arranged and well-ordered with minimal gaps between layers (Fig. 2c, e). In contrast, the foliated layers in shells under all three decreased pH treatments were less tightly packed and irregularly arranged (Fig. 2g, i, k, m, o and q). The area porosity of foliated layers was significantly increased by decreased pH treatments, regardless of older and younger shell (Older region: $F_{(3,11)} = 3.683$, $p = 0.045$;

190 Younger region: $F_{(3,11)} = 7.480$, $p = 0.005$) (Fig. 2r, s).

3.2 Decreased pH does not affect the crystallographic orientation of foliated layer

Electron backscatter diffraction (EBSD) intensity mapping analysis showed diffraction patterns for both calcite and aragonite crystals of older hinge regions in the juvenile shells (Fig. 3). From crystallographic orientation maps, though the foliated

layers of shells under decreased pH showed colour variations within a limited area (~ 5-10 foliated laminas) close to the interior, the majority of calcite crystal units showed uniform orientation, the same as those in the control (Fig. 3.i and ii). The spread of data points in the pole figures (Fig. 3.ii) confirmed the identical preferred crystallographic orientation of foliated layers, resulting in the extent of the variation in crystal orientation of 40 degree regardless of pH treatments, which corresponded to the colours in the orientation maps (Fig. 3.i). The aragonite crystal units appeared to be similarly distributed (Fig. 3.iii), but notably, there was an absence of aragonite in the shells formed under pH 7.2 (Fig. 3.iv). Though decreased pH had a restricted effect on the marginal foliated laminas closed to interior of oyster shell, the overall crystallographic orientation of main shell regions was not affected.

3.3 Decreased pH reduces shell mechanical properties

All decreased pH treatments significantly reduced the shell hardness when compared to shells in the controls (Fig. 4a, b) (Older region: $F_{(3,11)} = 21.987$, $p < 0.001$; Younger region: $F_{(3,11)} = 4.135$, $p = 0.034$). Similarly, shells at pH 7.5 and 7.2 had reduced Young's modulus compared to the controls (Fig. 4c, d) (Older region: $F_{(3,11)} = 4.525$, $p = 0.027$; Younger region: $F_{(3,11)} = 7.369$, $p = 0.006$). The reduced mechanical features due to decreased pH were observed in both the older hinge regions and younger middle regions (Fig. 4).

3.4 An overall "down-shifting" of shell density with decreased pH

Three-dimensional (3D) shell density maps, the overall shell density and mineral density-volume ratio relationships by micro-computed tomography (Micro-CT) showed an overall "down-shifting" of mineral density in the shell with decreasing pH (Fig. 5). The shell mineral density was significantly reduced by decreased pH (Fig. 5e) ($F_{(3,8)} = 5.318$, $p = 0.026$) which may be due to the altered mineral density-volume ratio relationships (Fig. 5f). Volume ratios were decreased with the increased mineral density in all pH treatments (ANCOVA; mineral density, $F_{(1,263)} = 1253.14$, $p < 0.001$). There was an interaction between pH and mineral density (ANCOVA; pH ×mineral density, $F_{(3,263)} = 4.994$, $p = 0.002$), indicating that the effect of pH on the mineral density-volume ratio was different. The lower scaling of consumptions at pH 7.8 (mean exponent -0.063), pH 7.5 (mean exponent -0.065), pH 7.2 (mean exponent -0.062) versus the control pH level of 8.1 (mean exponent -0.052), indicating the volume ratio of denser shell was reduced with decreased pH while the volume ratio of less denser shell was increased correspondingly (Fig. 5f). 3D shell density map (Fig. 5 a-d) reinforced the effect of decreased pH on the mineral density-volume ratio relationships. In the controls, shells were produced with denser minerals compared to shells in decreased pH (Fig. 5a). Shells in pH 7.8, pH.7.5 and pH 7.2 had larger proportions of lower mineral density regions or "pores" (Fig. 5b-d). These pores were observed in the 3D density maps as density values below the detection threshold (Fig. 5a-d). With classifying the shell volumes into four density categories, i.e., < 0.5 g/cm^3, 0.5-1 g/cm^3, 1-1.5 g/cm^3 and > 1.5 g/cm^3, the proportions of high (>1.5 g/cm^3) and low (< 0.5 g/cm^3) shell mineral density areas were significantly affected by decreasing pH (Fig. 5a-d). The volume ratios of high density areas were significantly reduced in all three decreased pH treatments (pH 7.8, pH 7.5 and pH 7.2) when compared to the controls ($F_{(3,8)} = 4.856$, $p = 0.033$). Meanwhile, the volume ratios of low density areas (< 0.5 g/cm^3) significantly increased in decreased pH treatments (pH 7.8, pH 7.5 and pH 7.2) when compared to the controls ($F_{(3,8)} = 6.945$, $p = 0.013$). There were no significant differences in the volume ratios of the middle mineral densities (0.5-1 g/cm^3: $\chi^2_{(2)} = 5.615$, $p = 0.132$; 1-1.5 g/cm^3: $F_{(3,8)} = 3.713$, $p = 0.061$) among treatments (Fig. 5a-d).

230 **4 Discussion**

This study provided new compiling information of structure - property relationships in calcareous shells of commercially important oyster species at different spatial scales and under a variety of environmentally and climatically relevant conditions of elevated CO_2 driven decreased pH. The reveled structural information and subsequent analysis of mechanical features in this study provided an important experimental basis for developing predictive models to forecast the impact of

235 ocean acidification process on marine calcifying organisms. The rate of calcareous shell formation of many marine organisms is expected to be significantly reduced in near-future oceans with a reduced pH of 7.8 due to ocean acidification (OA) process (Ries, 2011; Bednarsek et al., 2012). We have also observed a similar trend on calcification process in the *Crassostrea angulata* because decreased pH due to OA is not only depleting carbonate ions necessary for $CaCO_3$ mineralization, but also metabolically weakening marine organisms through the altered physiological processes, i.e. acidosis

240 (Dupont and Portner, 2013). Importantly, this study provided a strong evidence to support the argument that shells produced by oysters under OA are corroded with disorganized or impaired crystal orientation or microstructures with reduced mechanical properties. The possible mechanisms and consequences underlying such a negative effects of decreased pH on mechanics of shell structure are discussed in the following sections.

4.1 Effect of ocean acidification on shell mechanical features: a hierarchical analysis

245 In any given biologically formed materials, mechanical properties at macroscale is generally depends on composition of material component and materials micro-structural features (Rodriguez-Navarro et al., 2002). In this study, oyster shell material is composed of two inorganic $CaCO_3$ compounds, calcite and aragonite. Oysters begin their life (larvae) with aragonite-based shell, but it is completely replaced by calcite in adults though juvenile shells may retain a tiny portion of aragonite. Calcite is a relatively less soluble form of $CaCO_3$ to decreased environmental pH when compared to aragonite.

250 This chemical feature of calcite may have made feasible for the juvenile oysters to successfully mineralize and retain the laminated calcareous structure even under undersaturated $CaCO_3$ saturation levels, e.g. decreased pH 7.4 (Fig. 2).

Like a previously described oyster shell microstructure, the materials used in this study composed of structurally organized layers. The bulk of the microstructure is characterized by the foliated layer with laminated lamellar structure of crystal units. In order to understand the modulating effect of environmental pH on the relationship between the shell

255 structural and mechanical features, we have quantified the "space or gap or pore" size between laminated layers within the folia. The decreased pH significantly increased size and quantity of the pore in the folia layer. The presence of such a loosened laminated folia with pores or gaps was an obvious impairment of decreased pH. This micro-structural impairment was observed even under the near-future level of decreased pH 7.8, where the porosity was increased by 10 folds (Fig. 2r). On the other hand, the preferred orientation of crystal units within the folia layer showed no difference in all decreased

260 pH treatments, with *c*-axis of calcite units approximately perpendicular to the outer and inner shell surface. Nevertheless, hardness and stiffness of the folia layer were significantly reduced under decreased pH, possibly due to the impaired microstructure with significantly higher pore size and numbers.

Furthermore, we have measured the impacts of decreased pH on whole shell mineral density and thus on "pores or gaps" in foliated layers using micro-CT analysis. Notably, higher density mineral volume has started reducing with

265 decreasing pH. This result supports our finding on the effect of decreased pH on microscale structure and mechanical features in the folia. Calcite shell materials are brittle in nature, like egg shells or ceramics, therefore their resistance to deformation (or breaking force) is largely depend on stiffness parameter of the shell. Here, we have found that both the hardness and stiffness of the folia layer has started to reduce with decreasing pH, which may have triggered shell failure phenomenon under stimulated external attack. Under the condition of same external forces, the folia layer with lower

270 stiffness and hardness owing to loosened laminated micro-structure under decreased pH is expected to be highly vulnerable to predatory attack even though the preferred orientation of the brittle material (i.e. calcite) is unaffected (Kemeny and Cook, 1986). In addition, the overall "down-shifting" of mineral density detected by Micro-CT analysis indicates the loosed internal microstructure may run through the juvenile shell with decreasing pH, thus the above conclusion may be applicable for the entire oyster shell. In other words, the juvenile oyster shell with impaired

275 microstructural features is more prone to predator attack under near-future level of decreased pH due to OA processes.

4.2 Effect of ocean acidification on shell microstructure and crystallography

The outermost prismatic layers of the older hinge and younger middle regions was completely disappeared when juvenile oysters exposed to the extreme, but still environmentally and climatically relevant, the decreased pH of 7.2 with calcite undersaturation ($\Omega_{cal} \approx 0.66$) (Fig. 1h and Fig. 2n, p). This may be because of the corrosive effect of the calcite-

280 undersaturated seawater in the environment (Bednarsek et al., 2012). Similar impacts were observed in the juvenile scallop (pH 7.8 and pH 7.5), *Argopecten irradians* (Talmage and Gobler, 2010), juvenile hard-shell clams (pH 7.7), *Mercenaria mercenaria* (Dickinson et al., 2013) and the rock oyster (pH 7.8 and pH 7.6), *Saccostrea glomerata* (Watson et al., 2009).

The juvenile oysters exposed to decreased pH exhibited loosened microstructure in foliated layers (Fig. 2). Firstly, it may be due to the decreased calcification rate resulted from the metabolic depression and/or energy shortage in the decreased

285 pH conditions (Gobler and Talmage, 2014; Lannig et al., 2010). Secondly, the dissolution of the newly formed minerals of the inner surface in the decreased pH conditions may be another probable reason (Melzner et al., 2011). Based on the calcification mechanism of mollusc, undersaturated calcite conditions may be in contact with the inner shell surface (Addadi et al., 2006; Thomsen et al., 2010), where the newly formed minerals grow as the structural building blocks for foliated layers, in the decreased pH conditions. Thus, the newly formed minerals may still be prone to dissolution. When the

290 dissolution rate is faster than the calcification rate, organisms may tend to produce loosened microstructure of foliated layers. Similarly, mussel shells grown in decreased pH conditions (pH 7.65) showed inner shell surface dissolution (Melzner et al., 2011) and impaired shell microstructure (Hahn et al., 2012), which were consistent with the results in this study. The crystallography of marine shell is the other important proxy to environmental stressors (Milano et al., 2017). Compared to calcite, aragonite occupies much less amount of oyster shells and is more soluble under decreased pH conditions (Fitzer et al.,

295 2014). Therefore, because of the same reasons discussed above, an absent of aragonite in the older hinge regions at pH 7.2 (Fig. 3.iv) is observed in this study. A similar absence of aragonite also was reported in mussel shells in high pCO_2 (1000 μatm) conditions (Fitzer et al., 2014). Nevertheless, the aragonitic portion in the adult oyster shell is insignificant and it plays no role in determining the ultimate mechanical properties of the calcite predominant adult shells.

4.3 Ecological implications and conclusion

300 Although previous studies showed that early larval life stages of several edible oyster species were relatively physiologically tolerant to the near-future pH 7.8 due to OA (Dineshram et al., 2013; Ko et al., 2013; Ko et al., 2014), this study shows that they are still vulnerable due to the softer and less stiff shells in decreased pH conditions. Similar negative impact of OA on shell mechanical properties was reported in various marine calcifiers. For example, the pearl oyster, *Pinctada fucata*, produced a 25.9% weaker shell after exposure to acidified seawater at pH 7.8 (Welladsen et al., 2010). Decreasing shell

305 hardness in decreased pH conditions was also observed in the California mussel (pH 7.95 and pH 7.75)*, Mytilus californianus* (Gaylord et al., 2011), the hard clam (pH 7.7), *Mercenaria mercenaria* (Dickinson et al., 2013; Ivanina et al., 2013), and the serpulid tubeworm (pH 7.8), *Hydroides elegans* (Li et al., 2014). However, the effects of increased pCO_2 on shell mechanical properties are species-specific. Near-future decreased pH 7.8 did not affect shell hardness in the sea urchin

Paracentrotus lividus (Collard et al., 2016) or in the barnacle *Amphibalanus amphitrite* (McDonald et al., 2009). Indeed,
310   juvenile oysters of *C. gigas* significantly increased their shell strength and size as a compensatory adaptive response to the high pCO_2 condition (i.e., pCO_2 1000 µatm) (Wright et al., 2014), and the blue mussel, *Mytilus edulis*, produced a stiffer and harder calcite layer under in increased pCO_2 condition (i.e., pCO_2 1000 µatm) (Fitzer et al., 2015).

       The long-term survival strategy of oysters with mechanical softer and less stiff shells as yet to be studied. However, as shown in a recent study (Sanford et al., 2014), it appears that the mechanically weaker shell will result in compromised
315   defence ability, thus lead to potential experience of increased predation which may act as a strong selective pressure for oysters in the decreased pH condition. Moreover, results from a recent study suggest that oysters with reduced and impaired calcification mechanisms have lower capability to repair their shells once natural damage occurs (Coleman et al., 2014). This hierarchical study revealed that the OA-induced decreased pH conditions may cause a bottom-up deterioration on oyster shells, thus pose a serious threat to oyster survival and the health of coastal oyster reef structures in the near-future ocean.
320   This biological effect of OA on shell structures and mechanical features should be incorporated to the coastal oceanographic biophysical models to accurately project the survival of oysters in near-future coastal oceans.

       Author contributions. Y.M. and T.V. conceived and designed the study. Z.G and H.Y. performed the nanoindentation test and contributed materials and analysis equipment. S.C.F. and M.C. performed the EBSD analyses and contributed analysis
325   equipment. Y.M. and A.U. performed the CO_2 propagation experiment. Y.M. and C.L. performed the SEM imaging. K.W.K.Y. contributed materials and analysis equipment for Micro-CT scanning. Y.M. analysed the data. Y.M. drafted the manuscript, V.B.S.C., and T.V. contributed to the revisions.

       Competing interests. The authors declare no competing or financial interest.
330

       Acknowledgments. The authors would like to thank Shu Xiao and Yu Ziniu of South China Sea Institute of Oceanology, Chinese Academy of Sciences (Guangzhou, China) for providing brood stocks for this work and for their assistance with the oyster larval culture. We acknowledge the University of Hong Kong-EMU facility for helping with the SEM analysis. Thanks to Y.Y. Chui (University of Hong Kong, HKU) for sectioning and Tony Liu for helping with the micro-CT work.
335   We thank Peter Chung of the Imaging Spectroscopy and Analysis Centre (ISAAC) of the School of Geographical & Earth Sciences, University of Glasgow for his support in the EBSD analyses.

       Funding. This work was supported by a grant from the HKSAR-RGC (No. 778309M). M.C. thank the Scottish Universities Life Science Alliance (SULSA) and the Scottish Funding Council for funding the Hong Kong: Scotland Collaborative
340   Research Partnership Award (2014_HK-Scot-0038). S.C.F. acknowledges the support of the University of Glasgow Principal's Early Career Mobility Scheme.

References

Addadi, L., Joester, D., Nudelman, F., and Weiner, S.: Mollusk shell formation: a source of new concepts for understanding biomineralization processes, Chem. Eur. J., 12, 980-987, 10.1002/chem.200500980, 2006.

Barton, A., Hales, B., Waldbusser, G. G., Langdon, C., and Feely, R. A.: The Pacific oyster, *Crassostrea gigas*, shows negative correlation to naturally elevated carbon dioxide levels: Implications for near-term ocean acidification effects, Limnol. Oceanogr., 57, 698-710, 10.4319/lo.2012.57.3.0698, 2012.

Bednarsek, N., Tarling, G. A., Bakker, D. C. E., Fielding, S., Jones, E. M., Venables, H. J., Ward, P., Kuzirian, A., Leze, B., Feely, R. A., and Murphy, E. J.: Extensive dissolution of live pteropods in the Southern Ocean, Nat. Geosci., 5, 881-885, 10.1038/ngeo1635, 2012.

Beniash, E., Ivanina, A., Lieb, N. S., Kurochkin, I., and Sokolova, I. M.: Elevated level of carbon dioxide affects metabolism and shell formation in oysters *Crassostrea virginica*, Mar. Ecol. Prog. Ser., 419, 95-108, 10.3354/meps08841, 2010.

Celenk, C., and Celenk, P.: Bone density measurement using computed tomography, in: Computed Tomography - Clinical Applications, edited by: Saba, L., InTech, Rijeka, Croatia, 123-136, 2012.

Coleman, D. W., Byrne, M., and Davis, A. R.: Molluscs on acid: gastropod shell repair and strength in acidifying oceans, Mar. Ecol. Prog. Ser., 509, 203-211, 10.3354/meps10887, 2014.

Collard, M., Rastrick, S. P. S., Calosi, P., Demolder, Y., Dille, J., Findlay, H. S., Hall-Spencer, J. M., Milazzo, M., Moulin, L., Widdicombe, S., Dehairs, F., and Dubois, P.: The impact of ocean acidification and warming on the skeletal mechanical properties of the sea urchin *Paracentrotus lividus* from laboratory and field observations, ICES J. Mar. Sci., 73, 727-738, 10.1093/icesjms/fsv018, 2016.

De Bodt, C., Van Oostende, N., Harlay, J., Sabbe, K., and Chou, L.: Individual and interacting effects of pCO$_2$ and temperature on *Emiliania huxleyi* calcification: study of the calcite production, the coccolith morphology and the coccosphere size, Biogeosciences, 7, 1401-1412, 10.5194/bg-7-1401-2010, 2010.

Dickinson, G. H., Ivanina, A. V., Matoo, O. B., Portner, H. O., Lannig, G., Bock, C., Beniash, E., and Sokolova, I. M.: Interactive effects of salinity and elevated CO$_2$ levels on juvenile eastern oysters, *Crassostrea virginica*, J. Exp. Biol., 215, 29-43, 10.1242/jeb.061481, 2012.

Dickinson, G. H., Matoo, O. B., Tourek, R. T., Sokolova, I. M., and Beniash, E.: Environmental salinity modulates the effects of elevated CO$_2$ levels on juvenile hard-shell clams, *Mercenaria mercenaria*, J. Exp. Biol., 216, 2607-2618, 10.1242/jeb.082909, 2013.

Dickson, A. G., and Millero, F. J.: A comparison of the equilibrium constants for the dissociation of carbonic acid in seawater media, Deep Sea Res. (I Oceanogr. Res. Pap.), 34, 1733-1743, 10.1016/0198-0149(87)90021-5, 1987.

Dineshram, R., Thiyagarajan, V., Lane, A., Yu, Z., Xiao, S., and Leung, P. T. Y.: Elevated CO$_2$ alters larval proteome and its phosphorylation status in the commercial oyster, *Crassostrea hongkongensis*, Mar. Biol., 160 2189-2205 10.1007/s00227-013-2176-x, 2013.

Doerner, M. F., and Nix, W. D.: A method for interpreting the data from depth-sensing indentation instruments, J. Mater. Res., 1, 601-609, 10.1557/JMR.1986.0601, 1986.

Duarte, C. M., Hendriks, I. E., Moore, T. S., Olsen, Y. S., Steckbauer, A., Ramajo, L., Carstensen, J., Trotter, J. A., and McCulloch, M.: Is ocean acidification an ppen-ocean syndrome? Understanding anthropogenic impacts on seawater pH, Estuar. Coast., 36, 221-236, 10.1007/s12237-013-9594-3, 2013.

Dupont, S., and Portner, H.: Marine science: Get ready for ocean acidification, Nature, 498, 429-429, 10.1038/498429a, 2013.

Feely, R. A., Orr, J., Fabry, V. J., Kleypas, J. A., Sabine, C. L., and Langdon, C.: Present and future changes in seawater chemistry due to ocean acidification., Geophys. Monogr. Ser., 183, 175-188, 10.1029/2005GM000337, 2009.

Fitzer, S. C., Cusack, M., Phoenix, V. R., and Kamenos, N. A.: Ocean acidification reduces the crystallographic control in juvenile mussel shells, J. Struct. Biol., 188, 39-45, 10.1016/j.jsb.2014.08.007, 2014.

Fitzer, S. C., Zhu, W., Tanner, K. E., Phoenix, V. R., Kamenos, N. A., and Cusack, M.: Ocean acidification alters the material properties of *Mytilus edulis* shells, J. R. Soc. Lond. Interface, 12, 10.1098/rsif.2014.1227, 2015.

Gaylord, B., Hill, T. M., Sanford, E., Lenz, E. A., Jacobs, L. A., Sato, K. N., Russell, A. D., and Hettinger, A.: Functional impacts of ocean acidification in an ecologically critical foundation species, J. Exp. Biol., 214, 2586-2594, 10.1242/jeb.055939, 2011.

Gobler, C. J., and Talmage, S. C.: Physiological response and resilience of early life-stage Eastern oysters (*Crassostrea virginica*) to past, present and future ocean acidification, Conserv. Physiol., 2, cou004, 10.1093/conphys/cou004, 2014.

Hahn, S., Rodolfo-Metalpa, R., Griesshaber, E., Schmahl, W. W., Buhl, D., Hall-Spencer, J. M., Baggini, C., Fehr, K. T., and Immenhauser, A.: Marine bivalve shell geochemistry and ultrastructure from modern low pH environments: environmental effect versus experimental bias, Biogeosciences, 9, 1897-1914, 10.5194/bg-9-1897-2012, 2012.

Ivanina, A. V., Dickinson, G. H., Matoo, O. B., Bagwe, R., Dickinson, A., Beniash, E., and Sokolova, I. M.: Interactive effects of elevated temperature and CO_2 levels on energy metabolism and biomineralization of marine bivalves *Crassostrea virginica* and *Mercenaria mercenaria*, Comp. Biochem. Physiol. A Mol. Integr. Physiol., 166, 101-111, 10.1016/j.cbpa.2013.05.016, 2013.

Kemeny, J., and Cook, N. G. W.: Effective moduli, non-linear deformation and strength of a cracked elastic solid, Int. J. Rock Mech. Min. Sci., 23, 107-118, 10.1016/0148-9062(86)90337-2, 1986.

Ko, G. W. K., Dineshram, R., Campanati, C., Chan, V. B. S., Havenhand, J., and Thiyagarajan, V.: Interactive effects of ocean acidification, elevated temperature, and reduced salinity on early-life stages of the Pacific oyster, Environ. Sci. Technol., 48, 10079-10088, 10.1021/es501611u, 2014.

Ko, W. K. G., Chan, B. S. V., Dineshram, R., Choi, K. S. D., Li, J. A., Yu, Z., and Thiyagarajan, V.: Larval and post-Larval stages of Pacific oyster (*Crassostrea gigas*) are resistant to elevated CO_2, PloS ONE, 8, e64147, 10.1371/journal.pone.0064147, 2013.

Lannig, G., Eilers, S., Portner, H. O., Sokolova, I. M., and Bock, C.: Impact of ocean acidification on energy metabolism of oyster, *Crassostrea gigas*-changes in metabolic pathways and thermal response, Mar. Drugs, 8, 2318-2339, 10.3390/md8082318, 2010.

Lee, S. W., Kim, Y. M., Kim, R. H., and Choi, C. S.: Nano-structured biogenic calcite: A thermal and chemical approach to folia in oyster shell, Micron, 39, 380-386, 10.1016/j.micron.2007.03.006, 2008.

Lee, S. W., Jang, Y. N., Ryu, K. W., Chae, S. C., Lee, Y. H., and Jeon, C. W.: Mechanical characteristics and morphological effect of complex crossed structure in biomaterials: fracture mechanics and microstructure of chalky layer in oyster shell, Micron, 42, 60-70, 10.1016/j.micron.2010.08.001, 2011.

Li, C., Chan, V. B. S., He, C., Meng, Y., Yao, H., Shih, K., and Thiyagarajan, V.: Weakening mechanisms of the serpulid tube in a high-CO_2 world, Environ. Sci. Technol., 48, 14158-14167, 10.1021/es501638h, 2014.

McDonald, M. R., McClintock, J. B., Amsler, C. D., Rittschof, D., Angus, R. A., Orihuela, B., and Lutostanski, K.: Effects of ocean acidification over the life history of the barnacle *Amphibalanus amphitrite*, Mar. Ecol. Prog. Ser., 385, 179-187, 10.3354/meps08099, 2009.

Medaković, D., Popović, S., Gržeta, B., Plazonić, M., and Hrs-Brenko, M.: X-ray diffraction study of calcification processes in embryos and larvae of the brooding oyster *Ostrea edulis*, Mar. Biol., 129, 615-623, 10.1007/s002270050204, 1997.

Mehrbach, C., Culberson, C. H., Hawley, J. E., and Pytkowicx, R. M.: Measurement of the apparent dissociation constants of carbonic acid in seawater at atmospheric pressure, Limnol. Oceanogr., 18, 897-907, 10.4319/lo.1973.18.6.0897, 1973.

Melzner, F., Stange, P., Trübenbach, K., Thomsen, J., Casties, I., Panknin, U., Gorb, S. N., and Gutowska, M. A.: Food supply and seawater pCO_2 impact calcification and internal shell dissolution in the blue mussel *Mytilus edulis*, PloS ONE, 6, e24223, 10.1371/journal.pone.0024223, 2011.

Milano, S., Schöne, B. R., Wang, S., and Müller, W. E.: Impact of high pCO_2 on shell structure of the bivalve *Cerastoderma edule*, Mar. Environ. Res., 119, 144-155, doi.org/10.1016/j.marenvres.2016.06.002, 2016.

Milano, S., Nehrke, G., Wanamaker Jr, A. D., Ballesta-Artero, I., Brey, T., and Schöne, B. R.: The effects of environment on *Arctica islandica* shell formation and architecture, Biogeosciences, 14, 1577-1591, 10.5194/bg-14-1577-2017, 2017.

Newell, R. I. E., Kennedy, V. S., and Shaw, K. S.: Comparative vulnerability to predators, and induced defense responses, of eastern oysters *Crassostrea virginica* and non-native *Crassostrea ariakensis* oysters in Chesapeake Bay, Mar. Biol., 152, 449-460, 10.1007/s00227-007-0706-0, 2007.

Oliver, W. C., and Pharr, G. M.: An improved technique for determining hardness and elastic modulus using load and displacement sensing indentation experiments, J. Mater. Res., 7, 1564-1583, 10.1557/JMR.1992.1564, 1992.

Perez-Huerta, A., Cusack, M., Zhu, W., England, J., and Hughes, J.: Material properties of brachiopod shell ultrastructure by nanoindentation, J. R. Soc. Lond. Interface, 4, 33-39, 10.1098/rsif.2006.0150, 2007.

Perez-Huerta, A., and Cusack, M.: Optimizing electron backscatter diffraction of carbonate biominerals-resin type and carbon coating, Microsc. Microanal., 15, 197-203, 10.1017/S1431927609090370, 2009.

Pierrot, D., Lewis, E., and Wallace, D.: MS Excel program developed for CO_2 system calculations, ORNL/CDIAC-105a. Carbon Dioxide Information Analysis Center, Oak Ridge National Laboratory, US Department of Energy, Oak Ridge, Tennessee, 2006.

Ries, J. B.: Skeletal mineralogy in a high-CO_2 world, J. Exp. Mar. Bio. Ecol., 403, 54-64, 10.1016/j.jembe.2011.04.006, 2011.

Rodriguez-Navarro, A., Kalin, O., Nys, Y., and Garcia-Ruiz, J. M.: Influence of the microstructure on the shell strength of eggs laid by hens of different ages, Br. Poult. Sci., 43, 395-403, 10.1080/00071660120103675, 2002.

Sanford, E., Gaylord, B., Hettinger, A., Lenz, E. A., Meyer, K., and Hill, T. M.: Ocean acidification increases the vulnerability of native oysters to predation by invasive snails, Proc. R. Soc. London, Ser. B, 281, 20132681, 10.1098/rspb.2013.2681, 2014.

Talmage, S. C., and Gobler, C. J.: Effects of past, present, and future ocean carbon dioxide concentrations on the growth and survival of larval shellfish, Proc. Natl. Acad. Sci., 107, 17246-17251, 10.1073/pnas.0913804107, 2010.

Team, R. C. D.: R: a language and environment for statistical computing. R Development Core Team, Vienna. 2013.

Teniswood, C. M. H., Roberts, D., Howard, W. R., Bray, S. G., and Bradby, J. E.: Microstructural shell strength of the Subantarctic pteropod Limacina helicina antarctica, Polar Biol., 39, 1643-1652, 10.1007/s00300-016-1888-z, 2016.

Thiyagarajan, V., and Ko, G. W. K.: Larval growth response of the Portuguese oyster (*Crassostrea angulata*) to multiple climate change stressors, Aquaculture, 370-371, 90-95, 10.1016/j.aquaculture.2012.09.025, 2012.

Thomsen, J., Gutowska, M. A., Saphörster, J., Heinemann, A., Trübenbach, K., Fietzke, J., Hiebenthal, C., Eisenhauer, A., Körtzinger, A., Wahl, M., and Melzner, F.: Calcifying invertebrates succeed in a naturally CO_2-rich coastal habitat but are threatened by high levels of future acidification, Biogeosciences, 7, 3879-3891, 10.5194/bg-7-3879-2010, 2010.

Thomsen, J., Haynert, K., Wegner, K. M., and Melzner, F.: Impact of seawater carbonate chemistry on the calcification of marine bivalves, Biogeosciences, 12, 4209-4220, 10.5194/bg-12-4209-2015, 2015.

Watson, S.-A., Southgate, P. C., Tyler, P. A., and Peck, L. S.: Early larval development of the Sydney rock oyster *Saccostrea glomerata* under near-future predictions of CO_2-driven ocean acidification, J. Shellfish Res., 28, 431-437, 10.2983/035.028.0302, 2009.

Weiner, S., and Addadi, L.: Design strategies in mineralized biological materials, J. Mater. Chem., 7, 689-702, DOI: 10.1039/A604512J, 1997.

Welladsen, H. M., Southgate, P. C., and Heimann, K.: The effects of exposure to near-future levels of ocean acidification on shell characteristics of *Pinctada fucata* (Bivalvia: Pteriidae), Molluscan Res., 30, 125-130, 2010.

Wright, J. M., Parker, L. M., O'Connor, W. A., Williams, M., Kube, P., and Ross, P. M.: Populations of Pacific oysters *Crassostrea gigas* respond variably to elevated CO_2 and predation by *Morula marginalba*, Biol. Bull., 226, 269-281, 10.1086/BBLv226n3p269, 2014.

Figures
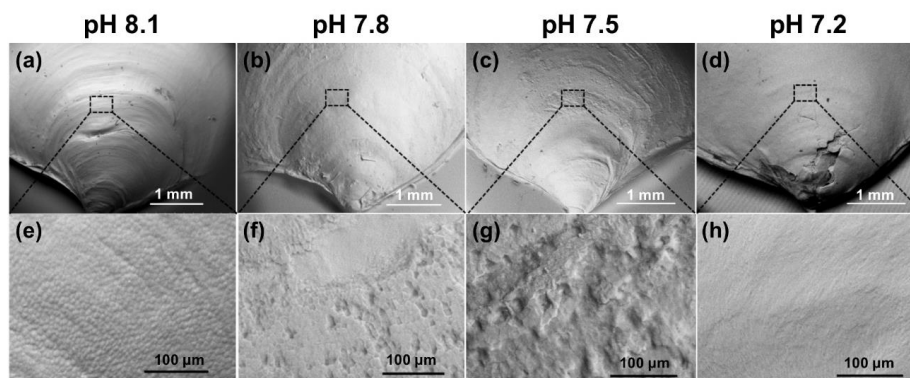
Figure 1: Scanning electron micrographs of 35-day-old juvenile *Crassostrea angulata* shells cultured at ambient or control pH 8.1 (a and e), treatment pH 7.8 (b and f), pH 7.5 (c and g) and pH 7.2 (d and h) were compared. Top row: low magnification tomography of the juvenile shells. Bottom row: enlarged view of the crystallite units (top view). (e) The prism units were arranged in compact prismatic structures at pH 8.1; (f) prismatic arrangement was partially lost at pH 7.8; (g) rough surface was observed demonstrating a much lower level of organization at pH 7.5; (h) a smooth surface was observed with no prismatic arrangement due to corrosion by environmental seawater.
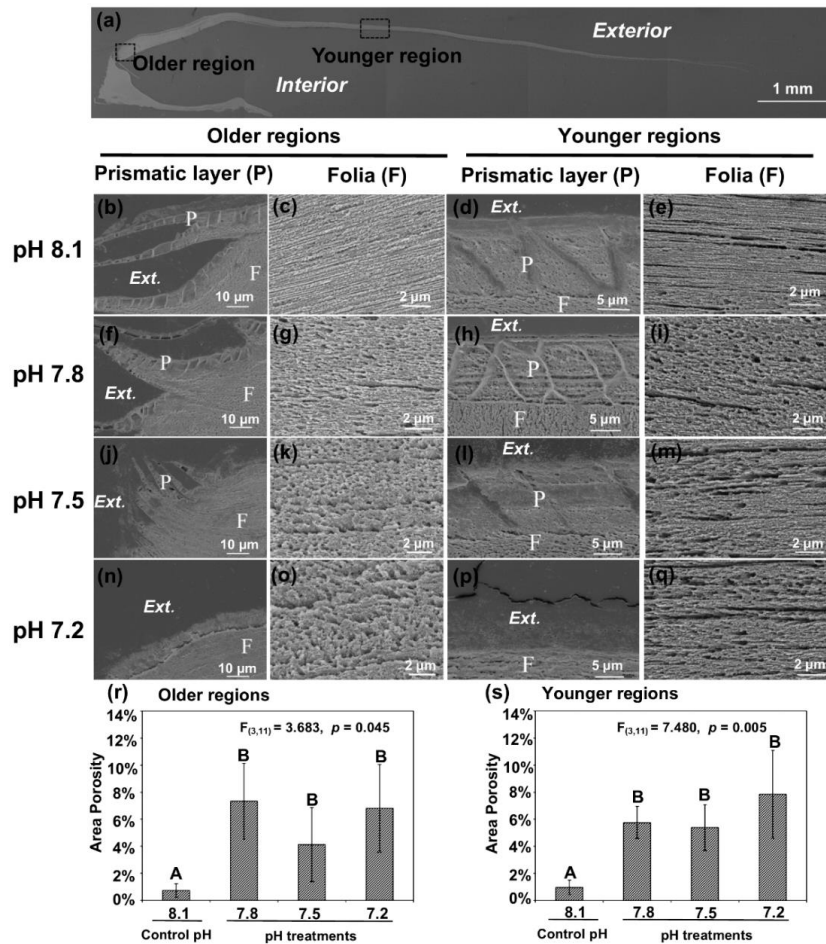
Figure 2: Microstructures were observed in the cross-sectional shell surfaces of 35-day-old juvenile *Crassostrea angulata*. Scanning electron micrographs were taken near the older hinge region (b, c, f, g, j, k, n and o) and the younger middle region (d, e, h, i, l, m, p and q). First row: scanning electron micrograph of the full shell cross-sectional surface (a). Second row: the prismatic layer (b and d) and tightly packed foliated structure (c and e) at pH 8.1. Third row: the prismatic layer (f and h) and the foliated structure with more and bigger pores (g and i) at pH 7.8 compared with at pH 8.1. Fourth row: the incomplete prismatic layer (j and l) and more porous foliated structure (k and m) at pH 7.5 compared with at pH 8.1. Fifth row: the prismatic layer was not detectable (n and p) with porous foliated structure (o and q) at pH 7.2. The porosity of foliated layers at the older (r) and younger regions (s) of the shell reared under control and low pH treatments. The mean values are presented in the bar chart (mean ± SD, n = 3 - 4). Annotations: P-prismatic layer; F- foliated layer.
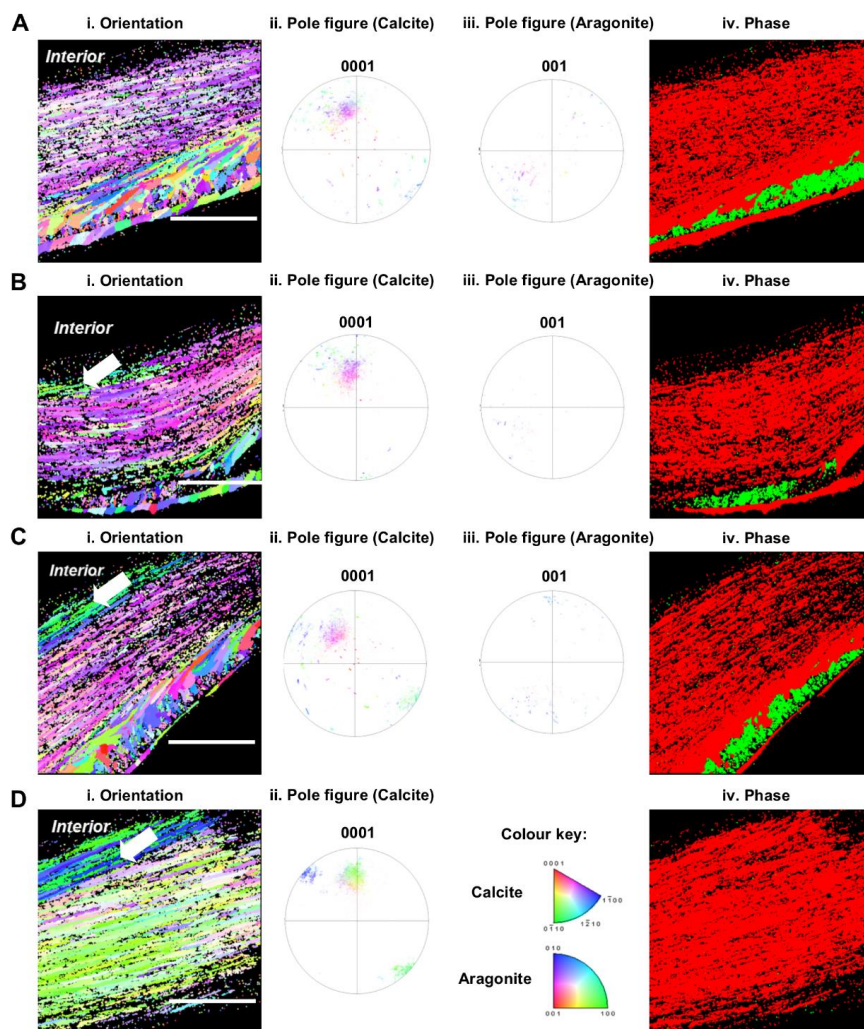
Figure 3: Electron Backscatter Diffraction analyses of shells grown for 35 days at control pH 8.1 (a), treatment pH 7.8 (b), pH 7.5 (c) and pH 7.2 (d). Crystallographic orientation maps (i) of calcite crystals in reference to the {0001} plane and aragonite crystals in reference to the {001} plane. Crystallographic planes of calcite are colour-coded according to the normal crystallographic direction shown in the colour key (Perez-Huerta and Cusack, 2009). Pole figures for calcite (ii) and aragonite (iii) corresponding to the crystallographic orientation maps with the same colour key. (iv) Phase map of calcite exhibited in red and aragonite in green. White arrow: change in colour of 5 to 10 marginal foliated laminates. Scale bar = 45 μm.
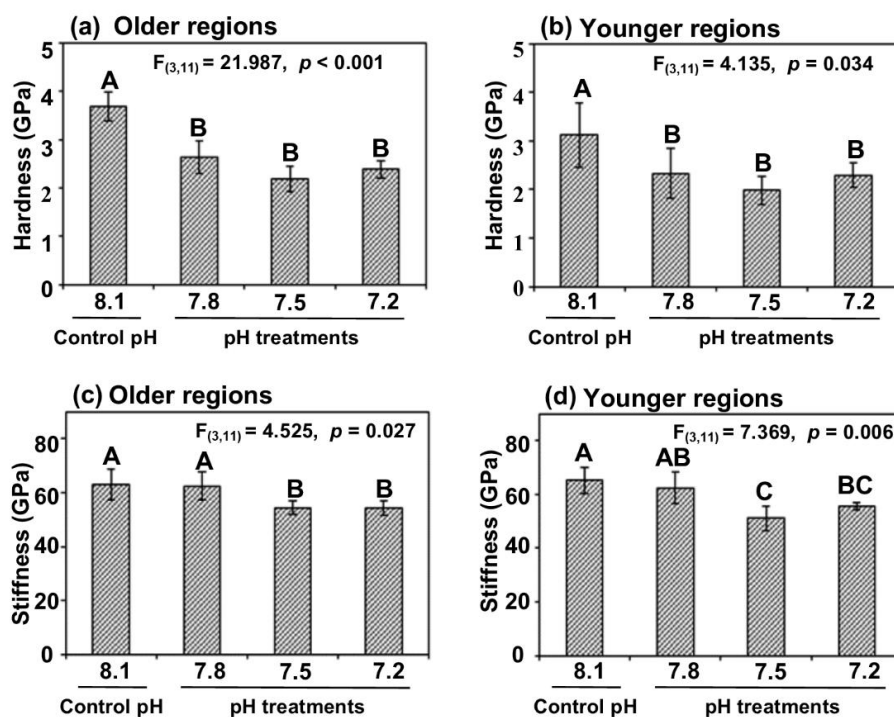
Figure 4: Shell mechanical properties in terms of hardness (a and b) and stiffness (c and d) with longer and shorter exposures in older hinge regions (a and c) and younger middle regions (b and d) in cross-sectional shell surfaces of *Crassostrea angulata* were compared. Data of mechanical properties are presented as mean ± SD of three to four replicates (n = 3 or 4).
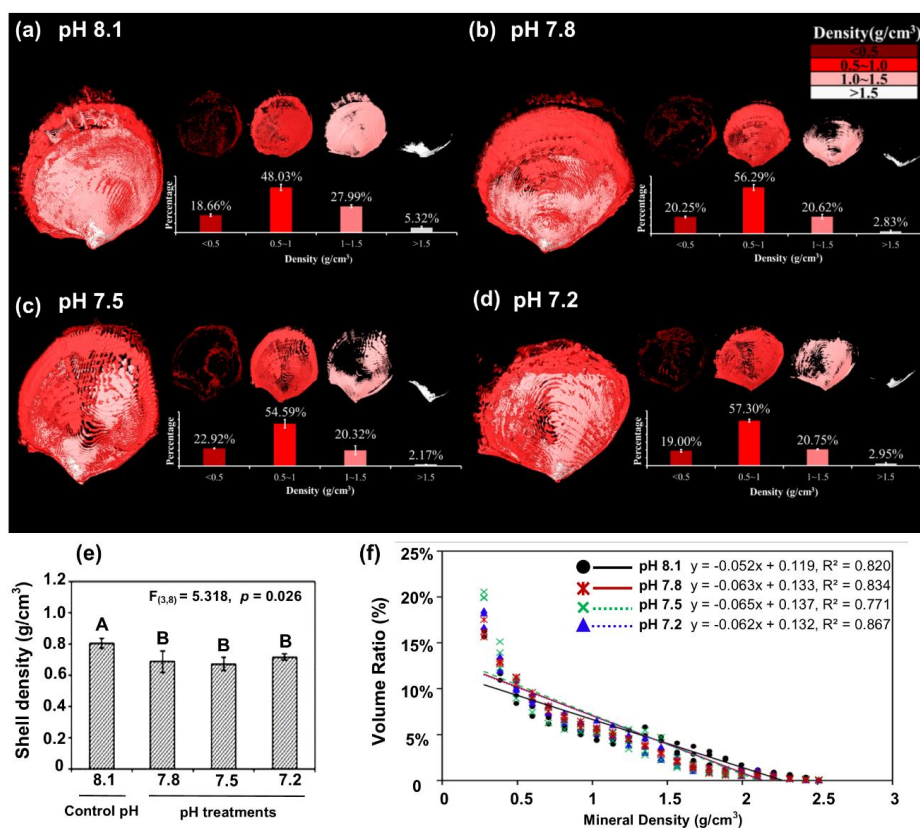
Figure 5: Effects of low pH on the shell density map (a-d), overall density (e), and mineral density - volume ratio relationships (f) for the four experimental pH treatment groups were examined by micro-CT of shells of *Crassostrea angulata*. Three dimensional reconstructions represent the density distribution of the shells produced in ambient or control pH 8.1 (a), treatment pH 7.8 (b), pH 7.5 (c) and pH 7.2 (d). The volume ratios of density categories of <0.5 g/cm³, 0.5-1.0 g/cm³, 1.0-1.5 g/cm³, and > 1.5 g/cm³ were quantified. (e) The overall density was presented as mean ± SD of three replicates (n = 3). (f) Mineral density–volume ratio relationships for the four experimental pH treatment groups of *C. angulata*. Regression lines for the three low pH treatments closely overlap and are partly obscured.